Constraining Cosmic Topology with CMB Polarization

Alain Riazuelo,[1,*] Samuel Caillerie,[2,†] Marc Lachièze-Rey,[2,‡] Roland Lehoucq,[2,§] and Jean-Pierre Luminet[3,¶]

[1] *Institut d'Astrophysique de Paris, 98bis boulevard Arago, F–75014 Paris, France*
[2] *CE-Saclay, DSM/DAPNIA/Service d'Astrophysique, F–91191 Gif-sur-Yvette Cedex, France*
[3] *Laboratoire Univers et Théories, CNRS-UMR 8102, Observatoire de Paris, F–92195 Meudon Cedex, France*

Multiply connected space sections of the universe on a scale smaller than the horizon size can leave an imprint on cosmic microwave background polarization maps, in such a way that the so-called "circles-in-the-sky" method can be used to detect or constrain the topology. We investigate some specific cases, namely toroidal and sixth-turn spaces, in order to show the influence of topology on CMB polarization. The correlation between matched points happens to be always positive and higher than 75% regardless of the angular scale and of the cosmological parameters, except for reionization. This figure is better than what occurs in temperature maps, but is achieved only in the absence of noise. It is only slightly reduced by the filtering scheme.

PACS numbers:

I. INTRODUCTION

The question of a possible multiply connected topology of our cosmic space goes back to the pioneering works of Schwarzschild and Friedmann more than 75 years ago. In the past two decades, various strategies and methods have been devised to probe a non trivial topology of the space sections of the universe, using current or forthcoming data from cosmological observations [1]. Since the topological length scales are a priori not known, it is useful to survey the largest observable scale in order to increase the odds of detecting, or at least constraining, the space topology. The Cosmic Microwave Background (CMB) emitting region, the so-called last scattering surface (LSS) is situated at a redshift of $z \simeq 1100$ and represents the deepest region that can be studied in the electromagnetic domain. Thus its usefulness for cosmology in general is tremendous [2]. Since more than one decade [3], temperature anisotropies in the CMB radiation have been mapped as a function of the direction. They result from density fluctuations in the primordial plasma, which are the seeds of evolved structures in the universe. Their study provides crucial information on the matter-energy contents of the universe, as well as some hints on the physical process which could have generated the first density perturbations at a much earlier epoch [2].

CMB anisotropies can also be used to constrain the topology. The main imprint of a non trivial topology on the CMB is well-known in the case when the characteristic topological length scale (called the injectivity radius) is smaller than the radius of the last scattering surface: the crossings of the LSS with its topological images give rise to pairs of matched circles of equal radii, centered at different points on the CMB sky, and exhibiting correlated patterns of temperature variations [4]. Such "circles-in-the-sky" searches are currently in progress using the WMAP data. They are however computationally very expensive, and present results are not completely clear. On the one hand, a massive search for matching circles with radii larger than 25° gave negative results [5]. But this result may well be overstated since, on the other hand, two other more specific searches gave hints for a positive detection. Roukema et al. [6] extended the search to smaller radii and claimed to have found six pairs of antipodal matched circles in a dodecahedral pattern; Aurich et al. [23] also found a marginal hint for spherical spaces, both searches being consistent with the Poincaré dodecahedron space model recently proposed by some of us [7] to account for the observed anomalies of the CMB angular power spectrum on large scales. The statistical significance of such results still has to be clarified. In any case, a lack of nearly matched circles does not exclude a multiply connected topology on scale less than the horizon radius: detectable topologies may produce circles of small radii which are statistically hard to detect and current analysis of CMB sky maps could have missed even antipodal matching circles because various effects may damage or even destroy the temperature matching [8, 9]. Moreover, even if it might already seem severely constrained

*Electronic address: riazuelo@iap.fr
†Electronic address: cailleri@discovery.saclay.cea.fr
‡Electronic address: marclr@discovery.saclay.cea.fr
§Electronic address: roller@discovery.saclay.cea.fr
¶Electronic address: jean-pierre.luminet@obspm.fr

by observational data, there are still unexpected and still unexplained features on the large angular scales of the CMB temperature map [10] which may hint for some sort of breaking in statistical isotropy of the CMB, a feature which is not shared by many models other than multiply connected topologies, and which is present even when the injectivity radius is larger than the size of the observable universe [8].

Recent work by Aurich *et al.* [9], Gundermann [11] and Caillerie *et al.* [12] support the dodecahedron model. Since the above mentioned anomalies detected in the first year WMAP data [10] suggest the presence of some statistical anisotropy in the CMB radiation, it appears thus necessary to better constrain topology, by using tests of different nature. It is now widely understood that the polarization of the CMB, predicted long ago [13], can provide a lot of additional informations for reconstructing the cosmological model [14]. The information encoded in polarization is expected to become a necessary input for precision cosmology, when it will be mapped in detail in the next release of the WMAP data [15] and later by the Planck satellite mission [16]. In this article we show how the polarization can also be used to put additional constraints on space topology.

This paper is organized as follows: in section II, we remind the key ingredients for detecting topological signatures in a CMB temperature map, using the circles-in-the-sky method. In section III, we recall the basic properties of CMB polarization that are useful for our purpose. We then compute in section IV the expected correlation for polarization maps, taking into account the specificities of polarization. Our main result is that the correlation in polarization maps is always larger than 75%, assuming an ideal case where no noise is present in the maps. In section V we present simulated maps for the 3-torus and the sixth-turn space in order to illustrate the validity of our method. In section VI, we look for various sources of blurring of the correlation when considering two effects: reionization and finite resolution.

II. CMB PHYSICS AND CORRELATION BETWEEN MATCHED POINTS IN TEMPERATURE MAPS

Let us first review the different contributions to CMB temperature as well as polarization anisotropies. The apparent temperature fluctuation in a given direction $\hat{\mathbf{n}}$ can be expressed (in Newtonian gauge) by

$$\Theta(\hat{\mathbf{n}}) \equiv \frac{\delta T}{T}(\hat{\mathbf{n}}) = \left(\frac{1}{4}\frac{\delta\rho}{\rho} + \Phi\right)\Big|_{r\hat{\mathbf{n}}} - \hat{\mathbf{n}}.\mathbf{v}_e(r\hat{\mathbf{n}}) + \int_0^r (\dot{\Phi} + \dot{\Psi})\Big|_{l\hat{\mathbf{n}}} \mathrm{d}l, \tag{1}$$

where the quantities Φ and Ψ are the usual Bardeen potentials [17], $\mathbf{v}_e$ being the velocity within the electron fluid. The first terms are evaluated at the LSS, i.e., at $r\hat{\mathbf{n}}$, where r represents the radius of the LSS. They represent the Sachs-Wolfe and Doppler contributions to CMB temperature anisotropies. The last term give accounts of the energy exchanged by photons with time-varying gravitational fields, known as the integrated Sachs-Wolfe (ISW) effect. This formula is independent of the topology of the universe and is valid in the limit of an infinitely thin last scattering surface and in absence of reionization. In order to go beyond these approximations, one should replace the quantities evaluated at the LSS, at $r\hat{\mathbf{n}}$, by quantities averaged on spheres of various radii, weighted by the probability for an electron to have experienced its last scattering at the corresponding epoch [18]. Such corrections are however not relevant for our purpose here.

In a multiply connected space, any two comoving points of space are joined by more than one geodesic. This characterizes the imprint of topology on cosmology. The immediate consequence is that the observed sky may show multiple images of a radiating source. Geometrically, the observational space identifies with the portion of the covering space (i.e. the corresponding simply connected manifold) which lies inside the horizon sphere. Multiple images (also called topological, or ghost images) of a given source are related by discrete isometries belonging to the holonomy group. The actions of these holonomies tile the observational space into identical cells which are copies of a fundamental domain. It results the most intuitive way to detect a multiply connected topology: to identify the multiple images of the same celestial object. This applies to faraway cosmological sources such as galaxy clusters [20] as well as spots in the CMB, i.e., different points of the LSS which would correspond to a single point of physical space.

When the fundamental domain is smaller than the size of the LSS (at least along one direction), the multiple images of the LSS so generated in the covering space intersect themselves. In this case, the Sachs-Wolfe contributions to the CMB radiation (which do not depend on the direction of observation) are strictly identical for homologous points of the LSS. This is at the basis of the now popular "circles-in-the-sky" method, since the intersection of two copies of the LSS sphere is a circle. Accordingly, a multiply connected topology may be characterized by temperature correlations between pairs of specific matched circles [4].

However, even in an ideal situation where noise removal would be perfect, such a correlation is not perfect. It is exact for the Sachs-Wolfe contribution (and even only on scales larger than the width of the last scattering surface), but absent for the Doppler and ISW contributions [8]. In particular, the ISW contribution depends on the whole

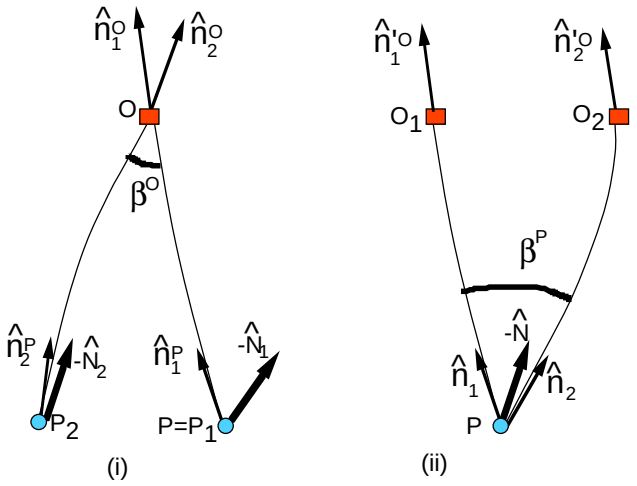

FIG. 1: Two points of view for describing the light-ray paths between a source point and the observer in a multiply connected space: (i) the observer O sees two images P_1 and P_2 of the same point of the last scattering surface; (ii) two copies of the observer, O_1 and O_2, see the same point P of the last scattering surface.

path between the emitting point of the LSS and the observer. In a multiply connected space, two matched points of the LSS are joined to the observer by two different paths. Therefore, their corresponding ISW contributions differ significantly, except possibly on the very largest scales. This blurs the temperature correlations.

A simple estimator for the correlation between pairs of circles, labelled by the two indices 1 and 2, is the *circle comparison statistics* (hereafter CCS) introduced by [4] as:

$$S(\phi_*) \equiv \frac{2 < \Theta_1(\pm\phi)\ \Theta_2(\phi+\phi_*) >}{< [\Theta_1(\pm\phi)]^2 + [\Theta_2(\phi+\phi_*)]^2 >} \tag{2}$$

where Θ_i is the temperature fluctuation along circle $i = 1, 2$, ϕ is the angle associated to the running point on the circles, and ϕ_* is the possible relative phase between the two circles. The average is done all along each circle, which means that $< >= 1/2\pi \int_0^{2\pi} \mathrm{d}\phi$. The $+$ sign in this equation correspond to phased circles and the $-$ sign to anti-phased circles arising in non-orientable topologies. With this set of notations, the CCS ranges in the interval $[-1, +1]$: circles that are perfectly matched have $S = 1$, while uncorrelated circles have a mean value of $S = 0$ and totally anti-correlated circles $S = -1$.

Let us for instance estimate the expected correlation of the Doppler contribution, which is the main term of blurring, in order to see the relative magnitude of the perturbation induced by this term on the total correlation. We will also suppose that the pairs of matched circles remain phased. This property occurs for instance when they are linked by a simple translation, like in the toroidal case. Without loss of generality, let us fix the coordinate system such that the two images of a point lie at colatitudes $\pm\alpha$ in directions $\hat{\mathbf{n}}_1 = (\sin\alpha, 0, \cos\alpha)$, $\hat{\mathbf{n}}_2 = (\sin\alpha, 0, -\cos\alpha)$. As seen in eq. (1), the amplitudes of the Doppler terms in these two directions are proportional to $\hat{\mathbf{n}}_1.\hat{\mathbf{N}}$ and $\hat{\mathbf{n}}_2.\hat{\mathbf{N}}$ respectively, where $-\hat{\mathbf{N}}$ represents the normalized direction of the electron fluid velocity (the same for both points according to our hypothesis). It results, between the two Doppler contributions, a correlation:

$$S_D = \frac{< 2\,\hat{\mathbf{n}}_1.\hat{\mathbf{N}} \times \hat{\mathbf{n}}_2.\hat{\mathbf{N}} >}{< (\hat{\mathbf{n}}_1.\hat{\mathbf{N}})^2 + (\hat{\mathbf{n}}_2.\hat{\mathbf{N}})^2 >}. \tag{3}$$

In the above equation, the average correlation is computed by averaging separately both the numerator and the denominator in the fixed direction $\hat{\mathbf{N}}$. After simple algebra, this gives

$$\langle S_D \rangle = -\cos(2\alpha) = \cos\beta, \tag{4}$$

where $\beta = \pi - 2\alpha$ represents the angular separation of the two points.

Can we generalise this reasoning to an arbitrary geometry and topology? In a multiconnected space, the observer O sees multiple images of an unique source point P in real space (Fig. 1, (i)). Let P_1 and P_2 be two images of the

same point source P. These images are of course related by $P_2 = g(P_1)$, where g is a holonomy transformation. The normalized direction of the velocity of the electron fluid is represented by $-\hat{\mathbf{N}}_\mathbf{1}$ at P_1 and $-\hat{\mathbf{N}}_\mathbf{2} = Dg(-\hat{\mathbf{N}}_\mathbf{1})$ at P_2, where Dg is the differential application corresponding to g. Two light rays reach the observer at O who can measure their arrival directions $\hat{\mathbf{n}}_1^O$ and $\hat{\mathbf{n}}_2^O$. A strict application of equation (3) would imply calculating the scalar products $\hat{\mathbf{n}}_1^O.\hat{\mathbf{N}}_\mathbf{1}$ and $\hat{\mathbf{n}}_2^O.\hat{\mathbf{N}}_\mathbf{2}$, hoping to express S_D in terms of observed quantities such as the angle β^O between $\hat{\mathbf{n}}_1^O$ and $\hat{\mathbf{n}}_2^O$ (it is well defined as $\cos\beta^O \equiv \hat{\mathbf{n}}_1^O.\hat{\mathbf{n}}_2^O$). But these scalar products are undefined because the vectors involved are not attached to the same point. Thus S_D must be better defined.

To generalise the reasoning to an arbitrary geometry and topology, we choose to adopt a dual point of view (Fig. 1, (ii)). The point source P, with velocity direction $-\hat{\mathbf{N}}$, emits light to two copies $O_1 = O$ and $O_2 = g^{-1}(O_1)$ of the observer. These two homologous observers see the source respectively in the directions $\hat{\mathbf{n}}_1'^O = \hat{\mathbf{n}}_1^O$ and $\hat{\mathbf{n}}_2'^O$, defined at O_1 and O_2 respectively. These two directions cannot be compared, nor their scalar product formed, since they correspond to vectors attached to different points of the covering space. However, the two light rays reaching O_1 and O_2 depart from the same point P following spatial directions $\hat{\mathbf{n}}_1$ and $\hat{\mathbf{n}}_2$. This allows us to apply equation (3) to estimate S_D as above. Averaging both the numerator and the denominator over $\hat{\mathbf{N}}$ gives $\langle S_D\rangle = \cos\beta^P$ where β^P defined by $\cos\beta^P \equiv \hat{\mathbf{n}}_1.\hat{\mathbf{n}}_2$ is the angle under which the source "sees" the two copies of the observer.

β^P is not an observable quantity. There is in principle no difficulty to convert β^P into β^O, but this is a tedious calculation, which requires the exact knowledge of the geometry of space and the explicit expression of the holonomy transformation g, and of its differential application Dg. This requires to estimate the parallel transport of the vectors $\hat{\mathbf{n}}_1$ and $\hat{\mathbf{n}}_2$ along the null geodesics (the light rays), as well as along the trajectory of the holonomy transformation. However, the situation is greatly simplified when space is flat: then $Dg = \mathrm{Id}$ for a translation, and $-\mathrm{Id}$ for a translation with space inversion. In this case, we have respectively $\cos\beta^P = \cos\beta^O$ and $\cos\beta^P = -\cos\beta^O$.

Unsurprisingly, two antipodal points are fully anticorrelated since they correspond to a Doppler effect seen from opposite directions, whereas the limit where the two points are in the same direction gives a fully correlated Doppler term. After a quick reminder about polarization in the next section, we shall perform a similar analysis for polarization.

III. A QUICK REMINDER OF CMB POLARIZATION

We recall that the propagation of a density wave in an anisotropic plasma induces a linear polarization of the CMB [13]. Each photon is polarized when scattered off by an electron of the photon-baryon plasma. The isotropic superposition of photons in the CMB destroys on the average the polarization. However, the presence of a local quadrupole in the photon fluid induces a weak residual polarization in the direction orthogonal to the plane defined by the quadrupole. The amount of *observed* polarization depends on the orientation of the observer with respect to the quadrupole, in analogy with the Doppler term dependence on the relative angle between the line of sight and the fluid velocity. The perfect fluid approximation for the photons would imply the absence of quadrupole. But, during the decoupling, the perfect fluid approximation is broken by the dramatic decrease of the scattering rate, as the free electrons become bound to the atomic nuclei. This generates a linear polarization of the CMB temperature. This prediction was only recently verified [21], because of the low amount of polarization expected.

To analyze the generation of polarization, we may consider a density wave, which generates density gradients in the photon fluid, in the direction of its wavevector. When the photons propagate, these density gradients generate a local dipole in the photon fluid: in a region initially richer in photons to its left than to its right, appears a dipole oriented from left to right. It results a dipole distribution, whose direction and intensity remain constant on a given waveplane, but vary along the orthogonal direction. A similar reasoning shows that this dipole gradient generates a local quadrupole, and so on. This is just a rewording of the Boltzmann equation, which couples the ℓ-th multipole of the radiation to the $(\ell-1)^{th}$ and $(\ell+1)^{th}$ multipoles.

Given such a local quadrupole, the scattering of photons on free electrons generates a polarization as explained above. Since the orientation of the dipole and quadrupole are determined uniquely by the direction of the initial density field, the generated polarization also depends on the angle between the line of sight and the quadrupole direction.

For convenience, the usual linear Q and U Stokes parameters, measured in each direction of the microwave sky (and assuming some rather arbitrary choice of the axis of the polarizer), are split into "electric" and "magnetic" parts, through a non local transformation. These names reflect the intuitive properties of the corresponding patterns with respect to parity transformation. For symmetry reasons, the density fluctuations create only E-modes (i.e. curl-free) polarization patterns on the sky. Although one expects that tensor modes (gravitational waves) also contribute to the CMB fluctuations, the scalar (density) modes are expected to be dominant [2]. Thus, we assume hereafter that polarization is due to scalar modes only, so that we only consider the angular dependence of the amplitude of the scalar E modes.

IV. CORRELATION IN POLARIZATION MAPS

The polarization is estimated by a method similar to that of Sec. II. The only difference lies in the angular dependence of the scalar part of the polarization tensor.

The amplitude of the temperature fluctuation due to the Doppler term is proportional to $\hat{\mathbf{n}}.\hat{\mathbf{N}} = \cos\theta$, where θ is the angle between the fluid velocity direction $\hat{\mathbf{N}}$ and the line of sight $\hat{\mathbf{n}}$. Thus, the total angular momentum method associates naturally the scalar part of this Doppler term with the spherical harmonics Y_1^0. In a similar way [14], one can associate the scalar part of the polarization with the spin-weighted spherical harmonics ${}_2Y_2^0 \propto \sin^2\theta = 1-(\hat{\mathbf{n}}.\hat{\mathbf{N}})^2$. Although far less intuitive, this can be understood from purely geometrical considerations as indicated in [14]. This allows us to compute the Doppler contribution of the expected correlation S_D^E of the scalar E mode of polarization for the two points, by a method similar as above: one simply has to replace in (3) the angular dependence $\hat{\mathbf{n}}.\hat{\mathbf{N}} = \cos\theta$ by $1-(\hat{\mathbf{n}}.\hat{\mathbf{N}})^2 = \sin^2\theta$. Therefore, one obtains:

$$S_D^E = \frac{< 2\,(1-(\hat{\mathbf{n}}_1.\hat{\mathbf{N}})^2) \times (1-(\hat{\mathbf{n}}_2.\hat{\mathbf{N}})^2) >}{< [1-(\hat{\mathbf{n}}_1.\hat{\mathbf{N}})^2]^2 + [1-(\hat{\mathbf{n}}_2.\hat{\mathbf{N}})^2]^2 >}, \tag{5}$$

and, after averaging,

$$S_D^E = 1 - \sin^2\alpha\cos^2\alpha = 1 - \frac{1}{4}\sin^2\beta \tag{6}$$

Thus, in the worst case (points in orthogonal directions), the correlation level still remains above 75%, whatever the value of β, and increases toward 1 for antipodal points. But β is the angle between the two copies of the observer as seen from the point source and is different from the observed angle β^O between the copies of the source as seen by the observer. Thus, formula (6) could not directly gives us the observed variations of S_D^E but indicates that the blurring due to the Doppler effect is always weak, more precisely that $S_D^E(\beta^O) \geq 0.75$, for all β^O as it is true for all β.

V. SIMULATED MAPS AND RESULTS

In order to illustrate the efficiency of the method, we apply it, as an example, to two simple cases of multiconnected flat spaces: the 3-torus and the sixth-turn space [8]. We consider a flat ΛCDM model with density parameters $\Omega_\Lambda = 0.7$, $\Omega_{\rm cdm} = 0.3$, and a Hubble constant $H_0 = 72$ km s^{-1} Mpc^{-1}; we neglect reionization. We used our CMB code to compute maps of the scalar CMB polarization E, with the method described in [8]. The only difference is that the quantities $\Theta_\ell(k,\eta)$ are replaced by their polarization counterparts $E_\ell(k,\eta)$.

For the 3-torus, low resolution maps are presented in Fig. 2. The main result is that the polarization fluctuations are always positively correlated, although not as perfectly as for the (academic) pure SW temperature map, as shown after in Fig. 3.

For the sixth-turn space we calculate the correlations between circles on various simulated CMB maps. For this space, the fundamental domain is an hexagonal prism. But along the direction of the prism, the different copies are not deduced from a translation (as it is the case for a torus), but from a screw motion defined as a translation composed with a $\pi/3$ rotation along the vertical axis (here corresponding to the direction of the prism and to the vertical direction in the maps). The observer sitting at the center of the prism expects to see pairs of matched circles at opposite latitudes. In each pair the circles are relatively twisted by an angle $n\pi/3$, where n is the number of screw motions one has to perform to go from one circle to the other. The prism height L is taken equal to one Hubble radius. This implies a radius of the observable universe $R_{\rm LSS} \sim 3.246$ Hubble radii. Therefore, we expect a series of matched circles at latitudes

$$\theta_n = \pm\arccos\left(n\frac{L}{2R_{\rm LSS}}\right), \tag{7}$$

with $1 \leq n \leq 6$. The twist between the circles of latitude $\pm\theta_n$ is

$$\varphi_n = n\frac{\pi}{3}. \tag{8}$$

Since for a sixth-turn space, both the direction of observation and the angular dependence of the emitting region are subject to the same screw motions, the above formula (6) remains valid. Fig. 4 compares the circle matching for a scalar polarization E map and a temperature map. The dependence of the matching of the circles as a function of their distance is more straightforward.

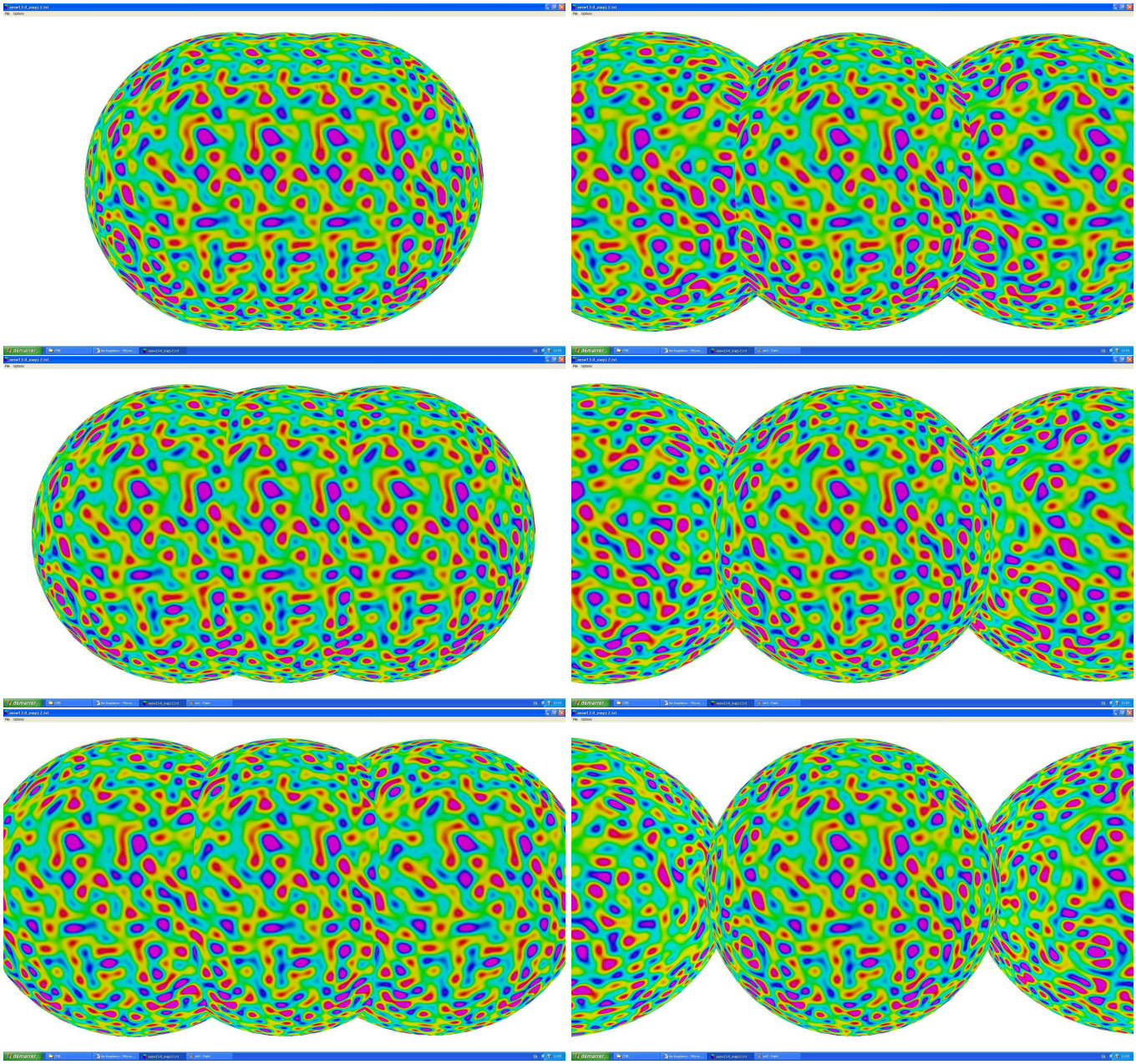

FIG. 2: The CMB scalar E polarization anisotropies in a flattened toroidal universe. We consider here a 3–torus with two lengths equal to the diameter of the LSS and one six times smaller (corresponding to the horizontal direction of the figure). We show three copies of the LSS along the small length, whose intersections correspond to the matched circles. We consider a small number of modes. No filtering has been applied to the map. Therefore, all the angular scales to which the modes contributes are faithfully represented here. The matching is very good for the largest nearby circles. It then decreases, and increases again for the smallest circles, as follows from Eq. (6). It is the worst case for circles of radius 45 degrees, as seen in the bottom left and upper right configurations.

VI. POSSIBLE SOURCES OF BLURRING OF THE CIRCLES

The nice result of Eq. (6) will however not correspond to what can be observed, at least for four reasons:

1. The relevance of Eq. (6) relies on the assumption that all the polarization is generated at the last scattering epoch, and does not take into account any equivalent of the ISW effect for the polarization. However, the duration of the last scattering epoch is short only in the absence of reionization. Since the last WMAP results [22] suggest that a significant amount of reionization took place, maybe as early as $z \sim 15$, one expects that some part of the

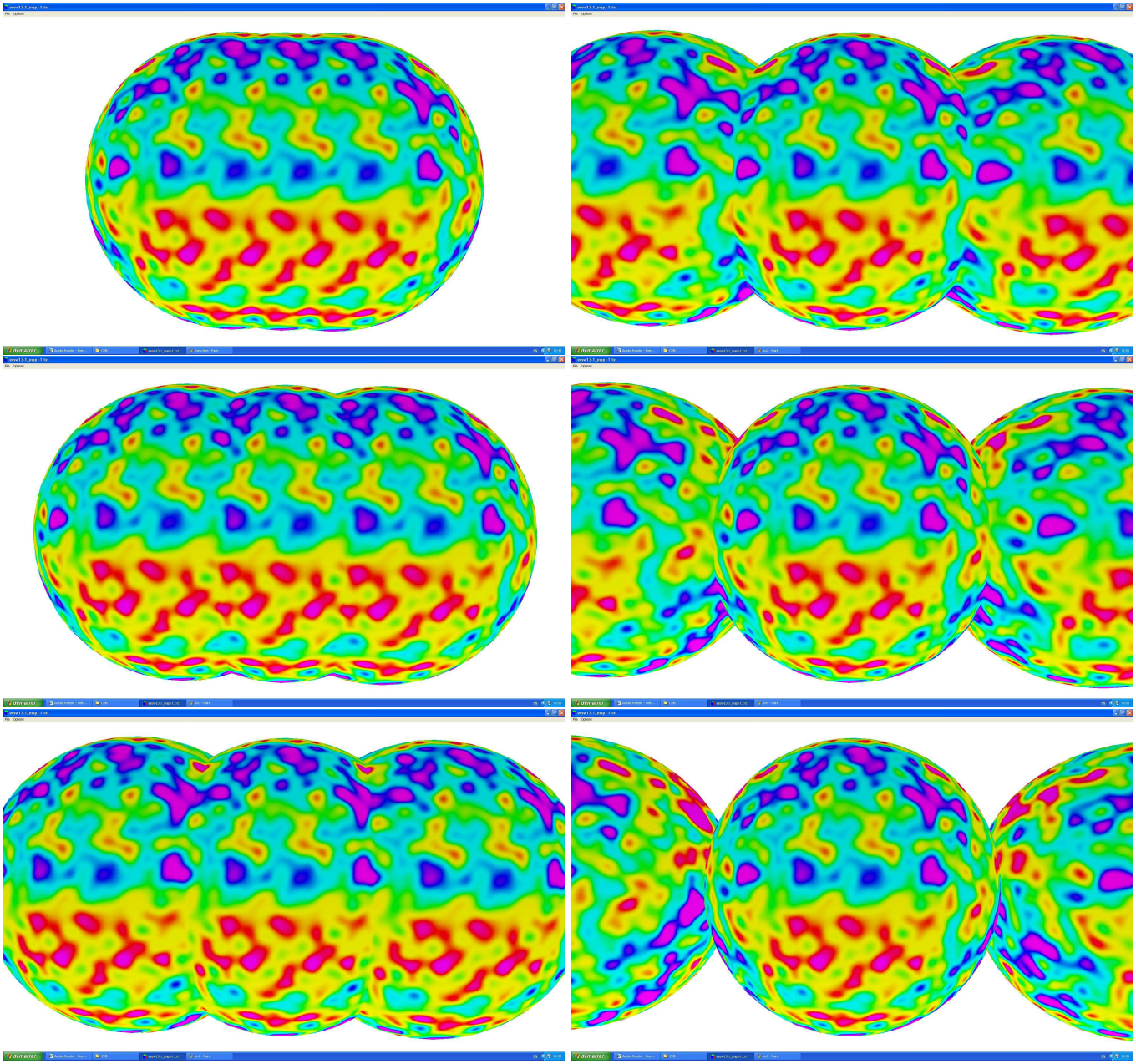

FIG. 3: Same as Fig. 2, but for the Sachs-Wolfe contribution. Since only the Sachs-Wolfe contribution is considered here, the matching between the circles is almost perfect, regardless of the angular size or distance of the circles. Note that the map seems to be at a lower resolution than the polarization map since the former has a relatively flat $\ell(\ell+1)C_\ell$ spectrum, whereas the latter has a fast growing spectrum because no large scale polarization is present.

observed CMB radiation was scattered long after recombination. This should induce a bump in the observed polarization spectrum at large angular scale (as well as a bump in the cross-correlated TE spectrum, as already claimed by the WMAP team). In this case, the angular scales at which reionization contributes should blur the circles. However, the angular power spectrum is strongly increasing in this region. Thus, at intermediate ($\ell \sim 60$) angular scales, the low ℓ contribution of reionization should become negligible, as compared to that of the recombination epoch.

2. Equivalently, gravitational lensing is expected to contribute to the CMB polarization anisotropies at large ℓ. The relevant range is however expected to be sufficiently different (large angular scales for reionization, small ones for lensing), as to preserve a limited range of ℓ where both reionization and lensing are negligible.

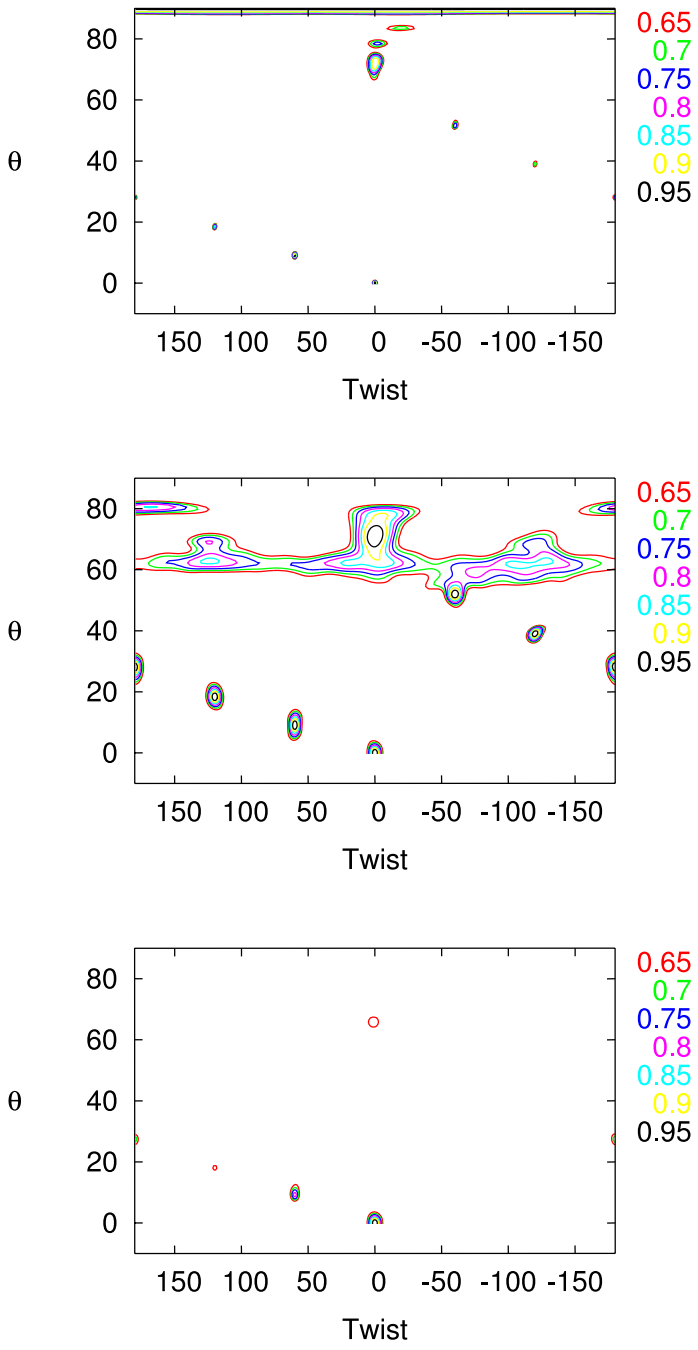

FIG. 4: Comparison of the circle matching for a scalar polarization E map and a temperature map. In these plots we compute the correlation between circles of latitudes $\pm\theta$, with a possible twist between them in a sixth-turn space. Given the small correlation length of CMB anisotropies in any realistic cosmological model, the correlation between circles is expected to be negligible except when the circles are very close (around $\theta = 0$ with a negligible twist), or for the values θ_n and φ_n given in Eq. (7)–(8) given by the topology we consider here. The first plot shows the correlation for a polarization map, whereas the next one shows the correlation for the pure Sachs-Wolfe effect, then the full temperature map for the same density field. Although the pure (but unobservable) Sachs-Wolfe contribution always gives as expected a 100% correlation (up to pixellization effects) for the matching circles, it is no longer the case for the other maps. Note that the correlation in the polarization map starts from 100% for untwisted equatorial circles, then decreases and reaches a minimum for circles of latitude ~ 40 degrees, and then increases again for smaller circles, as expected. This pattern is always present in polarization maps. For comparison, a temperature map may not show such a regular pattern, in particular at low or intermediate angular scales such as in these maps, where either the ISW or Doppler terms blur the correlations.

3. We have assumed a perfect signal-to-noise ratio in the data. This is certainly the most objectable hypothesis done here, since at present very little is known on how to extract as accurately as possible foreground polarized emission from CMB observations. A careful analysis of the expected signal-to-noise ratio of WMAP and Planck mission polarization maps and its imprint on the detectability of the topology of the universe should be performed and is left for future studies.

4. Finally, Eq. (6) was calculated under the assumption that the whole set of angular scales to which a plane wave (say) contributes was observed. In practice, an angular filtering is applied to a map, in particular to account for the instrument resolution. A single mode with comoving wavenumber k mostly contributes to the angular scale ℓ such that

$$\ell \sim k\eta_{\rm LSS}, \tag{9}$$

where $\eta_{\rm LSS}$ is the comoving distance of the last scattering sphere. However, this is only approximate, and a plane wave usually contributes also, although with less intensity, to all the angular scales larger than this value (see [18]). As a consequence, a map of resolution $\ell_{\rm max}$ exhibits in principle perfectly the correlations due to modes with $k \lesssim k_{\rm max} = \ell_{\rm max}/\eta_{\rm LSS}$, but also incompletely exhibits the contributions from larger wavenumbers. The consequence is a decrease of the expected correlation. To avoid this problem, the best way is to choose a value of $\ell_{\rm max}$ which corresponds to a decreasing part of the spectrum, making the contribution of higher wavenumbers $k > k_{\rm max}$ as small as possible. For this reason, in a pure Sachs-Wolfe map, the correlation obtained when the resolution corresponds to the decrease of the first peak ($\ell_{\rm max} \sim 300 - 400$) is better than the correlation taken before the first peak maximum ($\ell_{\rm max} \sim 150$). It happens that the most detailed circle searches in CMB temperature map [5, 23] were precisely performed at angular resolution $\ell \sim 400 - 500$, so that this possibly annoying problem was evaded.

In other words, there is the necessity to convolve the three-dimensional Fourier spectrum with some window function in order to project it on the celestial sphere and obtain the C_ℓ. This window function is not infinitely narrow as was done in the approximation of Eq. (9). However, the window function associated to the scalar E mode of polarization is in fact far more peaked than that of the Sachs-Wolfe contribution to temperature anisotropies, mainly because of the intrinsic angular dependence of the polarization [18]. Therefore, this effect does seem to be problematic for the imprint of topology in polarization maps.

As we explained, among these four problems, the third one is certainly the most serious. It is possible that even the Planck mission sensitivity to polarization will not increase the signal-to-noise ratio sufficiently enough to allow to search for the topology of the universe in that way. Future polarization designed experiments, however, should be able to do the job. The problem addressed in this paper represents an example of the required sensitivity that might be imposed when designing next generation CMB experiments.

VII. CONCLUSION

High precision experiments such as WMAP now give a clear outline of the cosmological model of our universe. Despite this tremendous success of modern cosmology, some old questions such as the shape of space are still unanswered. In this paper, we have described a new test to search for the topology of the universe using polarization maps. This test is rather ambitious as it necessitates clean data on the CMB polarization map. Given the advantages of the polarization maps which have been presented here, it appears highly likely that future missions with sufficient good signal-to-noise ratio (Planck, or some future polarization dedicated missions) will help bringing definitive conclusions about the question of cosmic topology.

Acknowledgments

The authors wish to thank Simon Prunet, Glenn Starkmann and Jean-Philippe Uzan for helpful discussions about CMB physics and topology of the universe. Most of the simulations presented here were performed on the MPOPM cluster of the Meudon Observatory computing center. A.R. wishes to thank Prof. Yin for enlightening discussions

about floating point arithmetics.

---

[1] M. Lachièze-Rey & J.-P. Luminet, Phys. Rep. **254**, 135 (1995); J. Levin, Phys. Rep. **365**, 251 (2002); M. J. Reboucas, astro-ph/0504365 ; T. Souradeep and A. Hajian, astro-ph/0502248.
[2] See for example A. R. Liddle & D. H. Lyth, *Cosmological Inflation and Large-Scale Structure*, Cambridge University Press, Cambridge, England (2000).
[3] G. F. Smoot *et al.*, Astrophys. J. **396**, L1 (1992).
[4] N. J. Cornish, D. N. Spergel & G. D. Starkman, Class. Quant. Grav. **15**, 2657 (1998).
[5] N. J. Cornish, D. N. Spergel, G. D. Starkman & E. Komatsu, Phys. Rev. Lett. **92**, 201302 (2004).
[6] B. Roukema *et al.* , Astron. Astrophys. **423**, 821 (2004).
[7] J.-P. Luminet, J. Weeks, A. Riazuelo, R. Lehoucq & J.-P. Uzan, Nature (London) **425**, 593 (2003).
[8] A. Riazuelo *et al.*, Phys. Rev. D **69** 103518 (2004); A. Riazuelo *et al.*, Phys. Rev. D **69**, 103514 (2004).
[9] R. Aurich, S. Lustig & F. Steiner, astro-ph/0412569.
[10] H. K. Eriksen *et al.*, Astrophys. J. **605**, 14 (2004); Erratum *ibid.* **609**, 1198 (2004); C. J. Copi *et al.*, Phys. Rev. D **70**. 043515 (2004); D. J. Schwarz *et al.*, Phys. Rev. Lett. **93**, 221301 (2004).
[11] J. Gundermann, astro-ph/0503014.
[12] S. Caillerie, M. Lachièze-Rey, A. Riazuelo, J.-P. Luminet & R. Lehoucq, in preparation.
[13] M.J. Rees, Astrophys. J. **153**, L1 (1968).
[14] W. Hu & M. White, New Astronomy, **2**, 323 (1997).
[15] WMAP website: http://map.gsfc.nasa.gov∼.
[16] Planck website: http://sci.esa.int/science-e/www/area/index.cfm?fareaid=17 .
[17] See for example V. F. Mukhanov, H. A. Feldman & R. H. Brandenberger, Phys. Rept. **215**, 203 (1992); R. Durrer, Fund. Cos. Phys. **14**, 209 (1994).
[18] W. Hu & M. White, Phys. Rev. D **56** 596 (1997).
[19] M. Lachièze-Rey & J.-P. Luminet, Phys. Rept. **254** 135 (1995).
[20] R. Lehoucq, M. Lachièze-Rey and J.-P. Luminet, Astron. Astrophys. **313** 339 (1996).
[21] J. Kovac *et al.*, Nature (London) **420**, 772 (2002).
[22] C. L. Bennett *et al.*, Astrophys. J. Suppl. **1**, 148 (2003).
[23] R. Aurich, S. Lustig and F. Steiner, M.N.R.A.S. under press, astro-ph/0510847.